HAL
open science

On power Jaccard losses for semantic segmentation

David Duque-Arias, Santiago Velasco-Forero, Jean-Emmanuel Deschaud, Francois Goulette, Andrés Serna, Etienne Decencière, Beatriz Marcotegui

To cite this version:

David Duque-Arias, Santiago Velasco-Forero, Jean-Emmanuel Deschaud, Francois Goulette, Andrés Serna, et al.. On power Jaccard losses for semantic segmentation. VISAPP 2021 : 16th International Conference on Computer Vision Theory and Applications, Feb 2021, Vienne (on line), Austria. hal-03139997

HAL Id: hal-03139997

https://hal.science/hal-03139997v1

Submitted on 12 Feb 2021

HAL is a multi-disciplinary open access archive for the deposit and dissemination of scientific research documents, whether they are published or not. The documents may come from teaching and research institutions in France or abroad, or from public or private research centers.

L'archive ouverte pluridisciplinaire **HAL**, est destinée au dépôt et à la diffusion de documents scientifiques de niveau recherche, publiés ou non, émanant des établissements d'enseignement et de recherche français ou étrangers, des laboratoires publics ou privés.

On power Jaccard losses for semantic segmentation

David Duque-Arias[1][a], Santiago Velasco-Forero[1][b], Jean-Emmanuel Deschaud[1][c], François Goulette[1][d], Andres Serna[2][e], Etienne Decencière[1][f] and Beatriz Marcotegui[1][g]

[1]*MINES ParisTech, PSL Research University, France*

[2]*Terra3D Research, Paris, France*

Keywords: Loss functions, Image segmentation, Jaccard loss, deep learning, U-net architecture.

Abstract: In this work, a new generalized loss function is proposed called *power Jaccard* to perform semantic segmentation tasks. It is compared with classical loss functions in different scenarios, including gray level and color image segmentation, as well as 3D point cloud segmentation. The results show improved performance, stability and convergence. We made available the code with our proposal with a demonstrative example.

1 INTRODUCTION

Image segmentation using learning-based approaches is an active research topic. One of the most common issues in this task is related to highly unbalanced datasets. Several strategies have been proposed in order to compensate less populated classes. They can be mainly clustered in two categories: *1)* Data-level methods, increasing artificially the number of training samples via *data augmentation* through over-sampling and under-sampling training samples; *2)* Algorithm-level methods, without modifying the training data distribution, the decision process increases the importance of smaller classes (Johnson and Khoshgoftaar, 2019). In this paper, we focus on the second approach, by modifying the loss function to penalize model mistakes similar to focal loss (Lin et al., 2017).

According to (Jun, 2020), loss functions can be mainly divided in two groups: **1)** *Statistical-based* such as Cross-Entropy (CE) and some of its variants such as Weighted CE (Ronneberger et al., 2015), distance map penalized (Calivá et al., 2019) that computes a mask based on pixels that are close to a given class, Focal loss and top K-loss (Wu et al., 2016) that drop pixels when they are too easy to classify, given a threshold parameter.

[a] https://orcid.org/0000-0002-2966-4922
[b] https://orcid.org/0000-0002-2438-1747
[c] https://orcid.org/0000-0002-6696-9354
[d] https://orcid.org/0000-0003-1527-2650
[e] https://orcid.org/0000-0003-2348-3079
[f] https://orcid.org/0000-0002-1349-8042
[g] https://orcid.org/0000-0002-2825-7292

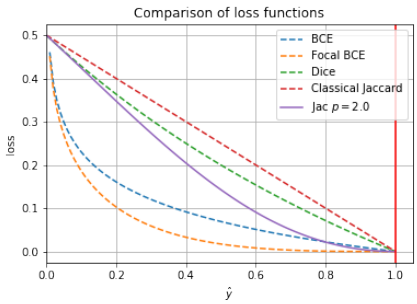

Figure 1: Comparison of some classical loss functions (dotted lines) and our proposed Power Jaccard loss (solid line). Binary Cross-Entropy. For Focal BCE with $\gamma = 2$. Vertical red line indicates the ground truth $y = 1$. Our proposal reduces the relative loss for well-classified examples.

2) *Geometrical-based* loss functions inspired by discrete sets and mostly motivated by Sørensen-Dice score. As an extension of Dice, Tversky loss (Salehi et al., 2017) allows to penalize differently False Positives (FP) and False Negatives (FN); well known Jaccard loss or Intersection over Union (IoU) (Polak et al., 2009) and its multiclass version *mean IoU*; boundary loss (Kervadec et al., 2018) takes the form of a distance metric in the space of contours. Penalty Generalized Dice (pGD) (Yang et al., 2019) seeks to penalize with an additional parameter both FP and FN. *Geometrical-based* loss functions are an active research field with successful results in semantic segmentation (Sudre et al., 2017).

During 3D point cloud challenge SHREC'20 (Zolanvari et al., 2019), we compared several losses to improve semantic segmentation (Ku et al., 2020). We found that some deep learning architectures such as Unet or SegNet (Badrinarayanan et al., 2017) did

not achieve high performance as expected, using the most common loss functions such as Focal loss, classical cross-entropy and Jaccard loss. Obtained results motivated us to propose a loss function able to penalize wrong predicted labels and to focus more on them to improve the general performance.

Our main contribution in this paper is a generalization of Jaccard loss function for image segmentation. In proposed loss, the higher the power term, the stronger the penalization of the worst predicted samples. We have evaluated our proposal with several segmentation datasets such as MNIST, Cityscapes (Cordts et al., 2016), SHREC'20 point clouds and aerial images (Mnih, 2013). The use of power losses improves the performance in binary and multiclass segmentation (section 4). Fig. 1 illustrates a comparison between the proposed loss functions and other classical losses as cross-entropy, Jaccard and Dice score. The abscissas represent the predicted value $\hat{y}$ and the ordinates the corresponding loss value. We will see that a higher value of p in our generalized Jaccard loss function improves model convergence by shifting the focus to improve harder predictions.

The structure of the paper is as follows: Section 2 describes the proposed loss function; Section 3 introduces the experimental design to evaluate our proposal; in Section 4 the results of semantic segmentation comparing several loss functions with different types of images are reported. Finally, in Section 5 the conclusions are stated.

2 LOSS FUNCTIONS

In this Section, we present power Jaccard loss generalizing the well known Jaccard index.

2.1 Jaccard index

The Jaccard index was introduced in (Jaccard, 1901). It measures the similarity measures the similarity between finite sample sets A, B as the Intersection over Union (IoU): $\frac{|A \cap B|}{|A \cup B|} = \frac{|A \cap B|}{|A|+|B|-|A \cap B|}$. The Jaccard index is zero if the two sets are disjoint and is one if they are identical. Other similarity index exist such as *Dice's index* defined as $\frac{2|A \cap B|}{|A|+|B|}$ and it can be rewritten in terms of Jaccard as $\frac{2J}{1+J}$. For minimization purposes, it is recommended to use the *Jaccard distance* $J_d = 1 - \frac{|A \cap B|}{|A \cup B|}$ a.k.a. Steinhaus distance or biotope distance, which were proposed to compare unordered sets (Deza and Deza, 2009). During the segmentation process, the loss function should evaluate each pixel i measuring the distance between its ground truth $y_i \in \{0,1\}$ and the current result of the model $\hat{y}_i$, the estimated probability value representing its likelihood of being part of the object. Subscript i is removed for simplification reasons in y_i and $\hat{y}_i$. The *straightforward* implementation of J_d as a loss function in continuous domain replaces intersection and union by product and sum as follows ((Rahman and Wang, 2016) and (Martire et al., 2017)):

$$J_1(y,\hat{y}) = 1 - \frac{(y \cdot \hat{y}) + \varepsilon}{(y + \hat{y} - y \cdot \hat{y}) + \varepsilon} \tag{1}$$

where ε prevents zero division.

(Cha, 2007) uses J_d as a variation of the normalized inner product to measure the distance between density probability functions with a power term equal to two in the denominator:

$$\begin{aligned} J_2(y,\hat{y}) &= 1 - \frac{(y \cdot \hat{y}) + \varepsilon}{(y^2 + \hat{y}^2 - y \cdot \hat{y}) + \varepsilon} \\ &= \frac{(y - \hat{y})^2}{(y^2 + \hat{y}^2 - y \cdot \hat{y}) + \varepsilon} \end{aligned} \tag{2}$$

This modification from (1) to (2) can be interpreted in the context of *focal loss*, where the main idea is to reduce both loss and gradient for correct prediction while emphasizing the gradient of errors (See Fig. 1).

2.2 Power Jaccard

We propose a generalized loss function called *Power Jaccard Loss* including a power term p to the Jaccard loss of (1) in order to increase the weight of wrong predictions during training, as follows:

$$J_p(y,\hat{y},p) = 1 - \frac{(y \cdot \hat{y}) + \varepsilon}{(y^p + \hat{y}^p - y \cdot \hat{y}) + \varepsilon} \tag{3}$$

If $p = 1$, our proposed loss is identical to Jaccard distance. Previous works have directly used $p = 2$ in geometrical losses such as Dice score (Diakogiannis et al., 2020) and Jaccard distance (Decencière et al., 2018).

Fig. 1 illustrates the shape of loss functions according to p. We propose to increase the weight of wrong predicted samples depending on p. Also, as shows Fig. 2 for $p > 2$, the minimum of loss function is not at $\hat{y} = 1$. This implies that the model will converge to a non desired optimal value and negative values of loss would be obtained. We also demonstrate that p must be between one and two.

3 EXPERIMENTAL DESIGN

Power Jaccard loss is validated in semantic segmentation frameworks with several datasets: MNIST,

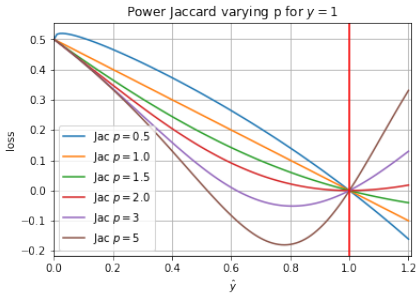

Figure 2: Incidence of parameter p in power Jaccard loss. Vertical red line indicates the ground truth value of $y = 1$.

Cityscapes, aerial images from Toronto University and SHREC'20 challenge. We selected Unet based architectures and performed some variations to the model (number of filters), the training stage (dataset size and batch size) and compared the incidence of our proposal. Each configuration is repeated several times to evaluate stability and repetitiveness, which is a common issue in neural networks (Scardapane and Wang, 2017). As evaluation metrics, we used mean IoU, accuracy and recall scores.

3.1 Grayscale images

MNIST dataset contains grayscale images of 28x28 pixels with digits of ten classes from zero to nine and one digit instance by image. We randomly selected 140 images per class and built a pixel-wise ground truth (Zhou, 2018). Then, the dataset was divided in the three common subsets as follows: 1000 for training, 200 for validation and 200 for test.

Two segmentation problems have been tackled: *1)* Binary segmentation to distinguish between background and digit pixels; *2)* Multiclass segmentation in ten classes. In both cases, we selected an Unet model with three levels of depth where the number of filters was changed between two, four and eight. Diverse batch sizes were used: 1, 10 and 50. Each configuration was evaluated with different losses: binary or categorical CE, classical Jaccard and power Jaccard with several values of p. In all trained models, the input shape is a single channel image. Each experiment is repeated five times. The code is available at [1].

3.2 RGB images

Two color datasets are used: *1)* Aerial images from (Mnih, 2013) for binary segmentation; *2)* Urban scenes images from Cityscapes (Cordts et al., 2016) for multiclass segmentation.

[1]The code to train a segmentation model on MNIST images varying the loss functions is available at: https://github.com/daduquea/powerLosses/.

(a) Road segmentation

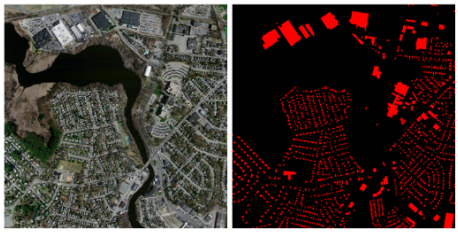

(b) Building segmentation

Figure 3: Example of Mnih dataset (RGB and GT).

3.2.1 Aerial images

We performed two binary segmentation tasks: *1)* Road and no-road (1108 images for training, 14 for validation and 49 for testing); *2)* Building and no-building (137 images for training, four for validation and ten for testing). Fig. 3 presents two images from the dataset and the corresponding ground truth.

Unet initialized from ImageNet with MobileNetV2 (Sandler et al., 2018) as feature extractor is used. Adam optimizer with a default learning rate of 10^{-3} and a patience equal to five.

3.2.2 Urban scene images

Cityscapes dataset is composed of 5K color images with divided in three subsets: training (2975), validation (500) and test (1525) and annotated with 30 classes in the context of autonomous driving. Fig. 4 shows an image from this dataset.

We have selected a subset of four classes relevant for autonomous driving to perform semantic segmentation in unbalanced data: person, car, road and background.

3.3 Point cloud projections

SHREC'20 dataset contains 80 point clouds, each one has about three millions points (x, y, z). Each point cloud of the training set is manually labeled with following classes: *building, car, ground, pole* and *veg-*

(a) RGB Image

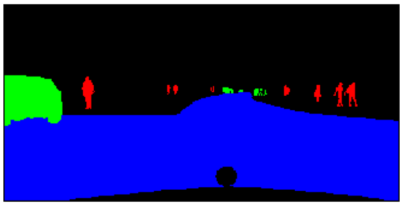

(b) Ground truth of selected classes. Color scale for each class: Road is blue, person is red, car is green and background is black.

Figure 4: Image from Cityscapes (Cordts et al., 2016).

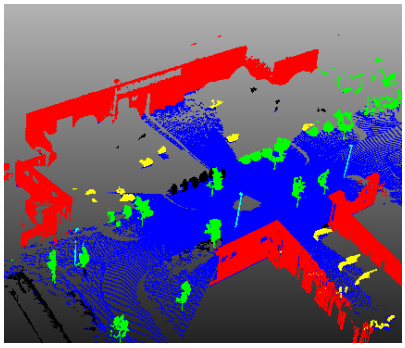

(a) 3D points

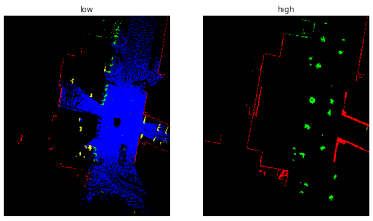

(b) Bird Eye View (BEV) projections

Figure 5: Point cloud with ground truth from SHREC'20 challenge (Zolanvari et al., 2019) and the corresponding BEV projections.

etation. Segmentation is obtained from 2D Bird eye view (BEV). Fig. 5 shows a point cloud with ground truth labels.

We divided segmentation of 3D point clouds in two simpler problems: **1)** Segment *lower* points (low slice) in *building* and *car* classes; **2)** Segment *higher* points (high slice) in *building* and *vegetation* classes. Fig. 5b shows BEV projections of *low* and *high slice* Fig. 5a.

Ground and *poles* have been discarded because: **1)** *Ground* can be extracted using an analytical approach such as the Lambda Flat Zone method proposed by (Hernández and Marcotegui, 2009) and then extended for (Serna and Marcotegui, 2014) to compute Digital Elevation Model (DEM); **2)** *Pole* class is problematic because a single traffic sign, very different from other pole instances, contains 70 % of the *pole* class points in the whole dataset.

We computed hand crafted features based on the BEV projections (Serna and Marcotegui, 2014) from 3D point clouds. For the low slice: h_{max} and $max(h_{max}, \Delta h_{min})$ and for the high slice: h_{min}, h_{max} and Δh. We note that h_{max} and h_{min} represent the maximum height and the minimum height of all points that fell in the same pixel, $\Delta h = h_{max} - h_{min}$ and $\Delta h_{min} = h_{min} - DEM$.

The semantic segmentation task was performed independently on each slice: one model was trained in the low slice and another one in the high slice. Both slices share some common characteristics such as the same Unet-based architecture with three levels of depth, the kernel size of convolutions, patience and Adadelta optimizer with a learning rate of 0.001.

4 RESULTS

In this section we present obtained results in binary and multiclass segmentation tasks. Power losses outperforms classical losses in tested scenarios with different kinds of data.

4.1 Gray scale images

4.1.1 Binary segmentation

Experiments with different number of filters, batch size and loss functions are performed. Table 1 shows the results using a batch size equal to one. Mean IoU, standard deviation and the best IoU of five runs are reported.

It was experimentally found that increasing the batch size negatively affects the performance of the model. It can be justified because with a smaller batch, the model gradually learns to distinguish between background and a single class. Even though, over a batch size of 10, the variance of the *digit* class increases because it groups a set on non homogeneous instances of the ten classes. Furthermore, Table 1 reports a high standard deviation for almost all config-

Filters	Metric	CE	Jac. p = 1
2	IoU	0.8542 ± 0.1651	0.4402 ± 0.0298
	Best IOU	0.9884	0.5000
4	IoU	0.8773 ± 0.1889	0.4551 ± 0.0366
	Best IOU	0.9878	0.5000
8	IoU	0.8216 ± 0.1654	0.4403 ± 0.0304
	Best IOU	0.9504	0.5011
Filters	**Metric**	**Jac. p = 1.25**	**Jac. p = 1.5**
2	IoU	0.5303 ± 0.2101	0.5538 ± 0.2217
	Best IOU	0.9507	0.9735
4	IoU	0.5545 ± 0.2234	0.5396 ± 0.2290
	Best IOU	**0.9977**	0.9566
8	IoU	0.4348 ± 0.0191	0.5395 ± 0.2290
	Best IOU	0.4737	**0.9977**
Filters	**Metric**	**Jac. p = 1.75**	**Jac. p = 2**
2	IoU	0.9813 ± 0.0172	0.7679 ± 0.2797
	Best IOU	**0.9977**	0.9975
4	IoU	0.6507 ± 0.2760	0.7687 ± 0.2804
	Best IOU	0.9938	**0.9977**
8	IoU	0.5397 ± 0.2289	0.5397 ± 0.2289
	Best IOU	**0.9977**	**0.9977**

Table 1: Binary segmentation in MNIST dataset with batch size of one

urations. It implies that during training, models converged to different local minima with different values at each run.

Power losses allow to train simpler models outperforming other loss functions. Table 1 shows that the model with two filters and power Jaccard with $p = 1.75$ obtained a performance equal to the best model with eight filters. The improvement obtained using power losses is higher when training smaller models. These loss functions could be useful with low memory requirements.

4.1.2 Multiclass segmentation

We varied batch size between 1, 10 and 50 and repeated five times each configuration, as presented in Table 2.

From Table 2, it can be seen that power Jaccard allows to obtain higher score compared against cross-entropy and classical Jaccard. Fig. 6 presents some predictions obtained with the best model achieved using power Jaccard with $p = 2$ and batch size of one. We observed that in the best models, the errors were in general at pixel-wise level. This type of errors can be solved by means of regularization techniques such as voting systems (Alpaydin, 1997).

4.2 RGB images

4.2.1 Aerial images

Table 3 presents accuracy values by experiment with several loss functions. We observe that in both experiments, the use of power losses leads to better results by a small margin and highest accuracy was obtained with $p = 1.5$. One may also note that BCE has the lowest validation accuracy in both datasets. The small differences between different loss functions occur because of to the use of an already trained model as feature extractor, as described in Section 3.

Batch	Metric	CE	Jac. p = 1
1	IoU	0.0956 ± 0.0309	0.0000 ± 0.0000
	Best IOU	0.1501	0.0000
10	IoU	0.1341 ± 0.0228	0.4537 ± 0.1014
	Best IOU	0.1612	0.6562
50	IoU	0.1534 ± 0.0101	0.4819 ± 0.0779
	Best IOU	0.1679	0.6188
Batch	**Metric**	**Jac. p = 1.25**	**Jac. p = 1.5**
1	IoU	0.0062 ± 0.0076	0.4831 ± 0.4031
	Best IOU	0.0152	0.9137
10	IoU	0.5298 ± 0.0963	0.6852 ± 0.0464
	Best IOU	0.6378	0.7747
50	IoU	0.5255 ± 0.1055	0.6364 ± 0.0699
	Best IOU	0.7342	0.7432
Batch	**Metric**	**Jac. p = 1.75**	**Jac. p = 2**
1	IoU	0.6388 ± 0.3394	0.5160 ± 0.4240
	Best IOU	0.8960	**0.9450**
10	IoU	0.8307 ± 0.0535	0.7953 ± 0.0499
	Best IOU	0.8793	**0.8856**
50	IoU	0.7403 ± 0.1137	0.7590 ± 0.0577
	Best IOU	**0.8342**	0.8064

Table 2: Mean IoU in multiclass segmentation on MNIST.

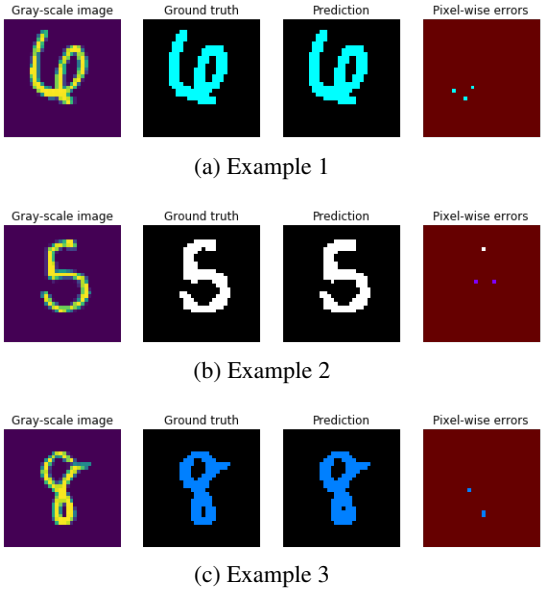

(a) Example 1

(b) Example 2

(c) Example 3

Figure 6: Multiclass segmentation using MNIST dataset. From left to right: *1)* Original gray scale image; *2)* Ground truth generated from gray scale image; *3)* Prediction using best obtained model; *4)* Errors between prediction and ground truth.

	Roads	Buildings
BCE	0.9622	0.9376
F-BCE	0.9677	0.9421
Dice	0.9680	0.9489
Jac. p = 1	0.9676	0.9484
Jac. p = 1.5	**0.9684**	**0.9503**
Jac. p = 2	0.9682	0.9502

Table 3: Accuracy in validation set on Aerial images. First column indicates the used loss function: BCE, Focal BCE, Dice score and power Jaccard.

	CE	Jac. p = 1	Jac. p = 1.5	Jac. p = 2
Person	0.1135	0.0000	0.1118	**0.1390**
Car	0.4620	0.4004	0.4209	**0.5082**
Road	**0.8380**	0.8137	0.8047	0.8263
Background	0.8721	0.8541	0.8605	**0.8738**
Mean IoU	0.5714	0.5170	0.5495	**0.5868**

Table 4: IoU by class and mean IoU in validation set of Cityscapes (Cordts et al., 2016).

4.2.2 Urban scene images

Table 4 reports the results on Cityscapes dataset. Power losses improve the performance on less populated classes such as person and car thanks to the higher penalty for worst predictions (see Fig. 2).

The *relative improvement* in IoU between cross-entropy and power Jaccard with p equal to 2 in *background* was 0.1949%, in *person* was 22.46% and in *car* was 10%. On the *road*, it worsened by 1.39%. In the *mean IoU*, the relative improvement was 2.69%. Fig. 7 shows the predictions of the image presented in Fig. 4 using the models trained with different losses. It is seen how the influence of the power term qualitatively improve the segmentation of the person class.

4.3 Point cloud projections

This section presents the results of semantic segmentation in 3D point clouds. We divide each point cloud in two slices: low and high, in order to simplify classification problems and focused on the impact of the loss function. Tables 5 and 6 present obtained results with several losses. We report three values by loss function: *IoU* is the average and the standard deviation of the mean IoU in test set and *best IoU* is the highest IoU obtained in test set

In general, using *Power Jaccard*, the performance

Metric	CE	Focal BCE	Dice score
IoU	0.279 ± 0.426	0.450 ± 0.172	0.665 ± 0.196
Best IOU	0.934	0.797	0.798
Metric	**Jac. p = 1**	**Jac. p = 1.5**	**Jac. p = 2**
IoU	0.702 ± 0.230	0.931 ± 0.009	0.925 ± 0.009
Best IOU	0.941	**0.943**	0.939

Table 5: Performance in low slice from SHREC'20 dataset.

(a) Cross-entropy

(b) Classical Jaccard

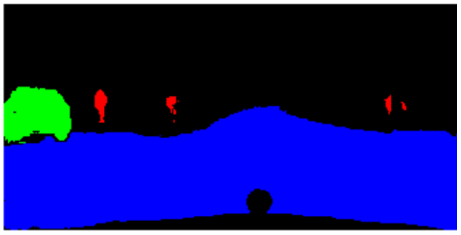

(c) Power Jaccard with $p = 1.5$

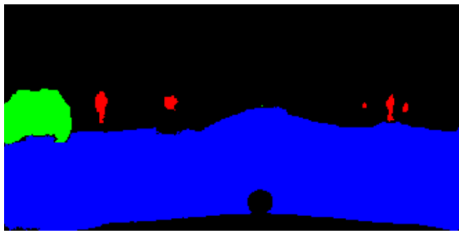

(d) Power Jaccard with $p = 2$

Figure 7: Example of Prediction 4 in Cityscapes. Road (blue), person (red), car (green) and background (black). Note that Power Jaccard performs better on smaller classes than the classical one. Quantitative results are given in Table 4

Metric	CE	Focal BCE	Dice p = 1
IoU	0.341 ± 0.000	0.570 ± 0.016	0.427 ± 0.173
Best IOU	0.341	0.605	0.787
Metric	**Jac. p = 1**	**Jac. p = 1.5**	**Jac. p = 2**
IoU	0.341 ± 0.000	0.761 ± 0.144	0.761 ± 0.020
Best IOU	0.341	**0.809**	0.788

Table 6: Performance in high slice from SHREC'20 dataset.

was better and the models converged more often. It can be seen by the low standard deviation values when p value increases, specially in the low slice results (Table 5). CE and Focal BCE do not converge as often as the proposed losses in tested scenarios. Even though, their best IoU in Table 5 is comparable with power functions. Models trained with $p = 1.5$ perform better than classical Jaccard in both slices.

5 CONCLUSIONS

In this work, we propose generalized loss functions to perform semantic segmentation by introducing power Jaccard. We evaluated it in different types of images such as gray-scale, RGB and point cloud projections in binary and multiclass segmentation tasks. Obtained results demonstrate that the use of power losses outperforms classical losses such as cross-entropy, Jaccard and Dice score.

In order to evaluate the stability of the models, we repeated several times the same configuration and we stated that the use of power losses helps to increase the rate of convergence. This is useful in deep learning models where the stability of the models is critical and it is strongly associated with the randomness of the initialization parameters.

We performed several experiments with different types of images, different dataset of segmentation task, demonstrating that the advantage of power losses is not an isolated case.

Additionally, to the results presented in this paper, we had conducted some experiments by including a power term in the classical Dice score in the same spirit of our proposal. Obtained results demonstrate that the use of p equal to two also improves the performance compared against the classical Dice loss in several scenarios. Accordingly, for future work, we will investigate a generalization of power terms on loss functions for semantic segmentation and a method to estimate the best value of p in different scenarios.

ACKNOWLEDGEMENTS

This work was partially funded by REPLICA FUI 24 project and ARMINES.

REFERENCES

Alpaydin, E. (1997). Voting over multiple condensed nearest neighbors. In *Lazy learning*, pages 115–132. Springer.

Badrinarayanan, V., Kendall, A., and Cipolla, R. (2017). Segnet: A deep convolutional encoder-decoder architecture for image segmentation. *IEEE transactions on pattern analysis and machine intelligence*, 39(12):2481–2495.

Calivá, F., Iriondo, C., Martinez, A. M., Majumdar, S., and Pedoia, V. (2019). Distance map loss penalty term for semantic segmentation. *arXiv preprint arXiv:1908.03679*.

Cha, S.-H. (2007). Comprehensive survey on distance/similarity measures between probability density functions. *City*, 1(2):1.

Cordts, M., Omran, M., Ramos, S., Rehfeld, T., Enzweiler, M., Benenson, R., Franke, U., Roth, S., and Schiele, B. (2016). The cityscapes dataset for semantic urban scene understanding. In *Proc. of the IEEE Conference on Computer Vision and Pattern Recognition (CVPR)*.

Decencière, E., Velasco-Forero, S., Min, F., Chen, J., Burdin, H., Gauthier, G., Laÿ, B., Bornschloegl, T., and Baldeweck, T. (2018). Dealing with topological information within a fully convolutional neural network. In *International Conference on Advanced Concepts for Intelligent Vision Systems*, pages 462–471. Springer.

Deza, M. M. and Deza, E. (2009). Encyclopedia of distances. In *Encyclopedia of distances*, pages 1–583. Springer.

Diakogiannis, F. I., Waldner, F., Caccetta, P., and Wu, C. (2020). Resunet-a: a deep learning framework for semantic segmentation of remotely sensed data. *ISPRS Journal of Photogrammetry and Remote Sensing*, 162:94–114.

Hernández, J. and Marcotegui, B. (2009). Point cloud segmentation towards urban ground modeling. In *2009 Joint Urban Remote Sensing Event*, pages 1–5. IEEE.

Jaccard, P. (1901). Distribution de la flore alpine dans le bassin des dranses et dans quelques régions voisines. *Bull Soc Vaudoise Sci Nat*, 37:241–272.

Johnson, J. M. and Khoshgoftaar, T. M. (2019). Survey on deep learning with class imbalance. *Journal of Big Data*, 6(1):27.

Jun, M. (2020). Segmentation loss odyssey. *arXiv preprint arXiv:2005.13449*.

Kervadec, H., Bouchtiba, J., Desrosiers, C., Granger, E., Dolz, J., and Ayed, I. B. (2018). Boundary loss for highly unbalanced segmentation. *arXiv preprint arXiv:1812.07032*.

Ku, T., Veltkamp, R. C., Boom, B., Duque-Arias, D., Velasco-Forero, S., Deschaud, J.-E., Goulette, F., Marcotegui, B., Ortega, S., Trujillo, A., et al. (2020). Shrec 2020 track: 3d point cloud semantic segmentation for street scenes. *Computers & Graphics*.

Lin, T.-Y., Goyal, P., Girshick, R., He, K., and Dollár, P. (2017). Focal loss for dense object detection. In *Proceedings of the IEEE international conference on computer vision*, pages 2980–2988.

Martire, I., da Silva, P., Plastino, A., Fabris, F., and Freitas, A. A. (2017). A novel probabilistic jaccard distance measure for classification of sparse and uncertain data. In de Faria Paiva, E. R., Merschmann, L., and Cerri, R., editors, *5th Brazilian Symposium on Knowledge Discovery, Mining and Learning (KDMiLe)*, pages 81–88.

Mnih, V. (2013). *Machine Learning for Aerial Image Labeling*. PhD thesis, University of Toronto.

Polak, M., Zhang, H., and Pi, M. (2009). An evaluation metric for image segmentation of multiple objects. *Image and Vision Computing*, 27(8):1223–1227.

Rahman, M. A. and Wang, Y. (2016). Optimizing intersection-over-union in deep neural networks for image segmentation. In *International symposium on visual computing*, pages 234–244. Springer.

Ronneberger, O., Fischer, P., and Brox, T. (2015). U-net: Convolutional networks for biomedical image segmentation. In *International Conference on Medical image computing and computer-assisted intervention*, pages 234–241. Springer.

Salehi, S. S. M., Erdogmus, D., and Gholipour, A. (2017). Tversky loss function for image segmentation using 3d fully convolutional deep networks. In *International Workshop on Machine Learning in Medical Imaging*, pages 379–387. Springer.

Sandler, M., Howard, A., Zhu, M., Zhmoginov, A., and Chen, L.-C. (2018). Mobilenetv2: Inverted residuals and linear bottlenecks. In *Proceedings of the IEEE conference on computer vision and pattern recognition*, pages 4510–4520.

Scardapane, S. and Wang, D. (2017). Randomness in neural networks: an overview. *Wiley Interdisciplinary Reviews: Data Mining and Knowledge Discovery*, 7(2):e1200.

Serna, A. and Marcotegui, B. (2014). Detection, segmentation and classification of 3d urban objects using mathematical morphology and supervised learning. *ISPRS Journal of Photogrammetry and Remote Sensing*, 93:243–255.

Sudre, C. H., Li, W., Vercauteren, T., Ourselin, S., and Cardoso, M. J. (2017). Generalised dice overlap as a deep learning loss function for highly unbalanced segmentations. In *Deep learning in medical image analysis and multimodal learning for clinical decision support*, pages 240–248. Springer.

Wu, Z., Shen, C., and Hengel, A. v. d. (2016). Bridging category-level and instance-level semantic image segmentation. *arXiv preprint arXiv:1605.06885*.

Yang, S., Kweon, J., and Kim, Y.-H. (2019). Major vessel segmentation on x-ray coronary angiography using deep networks with a novel penalty loss function. In *International Conference on Medical Imaging with Deep Learning–Extended Abstract Track*.

Zhou, L. (2018). M2NIST Segmentation / U-net.

Zolanvari, S., Ruano, S., Rana, A., Cummins, A., da Silva, R. E., Rahbar, M., and Smolic, A. (2019). Dublincity: Annotated lidar point cloud and its applications. *arXiv preprint arXiv:1909.03613*.

APPENDIX

Derivatives of Power Jaccard

As $y \in \{0,1\}$, the power term p does not affect y value. Eq. 3 can we rewritten as presented in Eq. 4. In order to find the minimum value of the loss function, we compute $\partial J_p / \partial \hat{y}$ and equaled to zero. We recall that $\hat{y} \in]0,1[$ because of the activation function. One may observe from Eq. 4 that $y = \hat{y} = 0$ results on zero division. Therefore, we suppose below that at least one of y and $\hat{y}$ are different from zero.

$$J_p(y,\hat{y}) = \frac{y + \hat{y}^p - 2 \cdot y \cdot \hat{y}}{(y + \hat{y}^p - y \cdot \hat{y})} \tag{4}$$

$$\frac{\partial J_p}{\partial \hat{y}} = \frac{(y \cdot \hat{y})(p \cdot \hat{y}^{p-1} - y)}{((y + \hat{y}^p - y \cdot \hat{y}))^2} - \frac{y}{(y + \hat{y}^p - y \cdot \hat{y})} \tag{5}$$

Let us consider the case where $y = 1$ so we replace it in Eq. 5 and solve to find the valid values for p based on the the minimum of the derivative of the loss function.

$$\frac{\partial J_p}{\partial \hat{y}} = 0$$

$$\frac{\hat{y} \cdot (p \cdot \hat{y}^{p-1} - 1)}{(1 + \hat{y}^p - \hat{y})^2} - \frac{1}{(1 + \hat{y}^p - \hat{y})} = 0$$

$$p \cdot \hat{y}^p - \hat{y} = 1 + \hat{y}^p - \hat{y} \tag{6}$$

If $p = 1$ there is not minimum as shows Fig. 1. But, if $p > 1$

$$\hat{y} = \sqrt[p]{\frac{1}{(p-1)}}$$

Note that $0 < \hat{y} < 1$, therefore:

$$0 < \frac{1}{(p-1)} < 1$$

$$1 < p < 2 \tag{7}$$

If $p = 2$, the minimum of Eq. 6 will be exactly at $\hat{y} = 1$. If $1 < p < 2$, the minimum of J_p beyond 2 which is not a problem as by construction $\hat{y}$ cannot be larger than 1. If $p > 2$, then the minimum will be between 0 and 1. Finally, if $p \leq 1$ there is no minimum.